Corrosion Science 167 (2020) 108488

Contents lists available at ScienceDirect

Corrosion Science

journal homepage: www.elsevier.com/locate/corsci

Degradation behavior of Ti-Nb alloys: Corrosion behavior through 21 days of immersion and tribocorrosion behavior against alumina

I. Çaha[a,*], A.C. Alves[a], P.A.B. Kuroda[b,c], C.R. Grandini[b,c], A.M.P. Pinto[a,d], L.A. Rocha[b,c], F. Toptan[a,b]

[a] CMEMS-UMinho - Center for MicroElectroMechanical Systems, Universidade Do Minho, Azurém, 4800-058, Guimarães, Portugal
[b] IBTN/Br, Brazilan Branch of the Institute of Biomaterials, Tribocorrosion and Nanomedicine, Bauru, SP, Brazil
[c] UNESP, Univ. Estadual Paulista, Faculdade de Ciências de Bauru, Dep. Física, 17033-360 Bauru, SP, Brazil
[d] Universidade do Minho, Dept. Eng. Mecânica, Azurém, 4800-058, Guimarães, Portugal

ARTICLE INFO

Keywords:
Titanium alloys
Biomaterials
Corrosion
Immersion
Tribocorrosion

ABSTRACT

Non-toxic and allergic free β-type Ti alloys are attractive metallic implant materials due to their lower Young's modulus and good biocompatibility, but the corrosion and tribocorrosion behavior are yet to be fully understood. In this study, corrosion behavior of Ti-15Nb and Ti-40Nb alloys was investigated and compared with the commercial Ti-6Al-4V alloy through an immersion period of 21 days. The tribocorrosion behavior was investigated under open-circuit potential by using a ball-on-plate tribometer. Results suggested that the β-type Ti-40Nb alloy having 51 GPa Young's modulus had lower corrosion and wear resistance as compared to the α + β-type Ti-15Nb and Ti-6Al-4V alloys.

1. Introduction

Ti and its alloys are the most attractive metallic biomaterials used in biomedical applications due to their high strength, excellent corrosion resistance and favorable biocompatibility. The α + β-type Ti-6Al-4V alloy has been widely used in orthopedic implants, particularly for total hip arthroplasties [1]. However, mostly used α-type and α + β-type Ti based implant materials have Young's modulus around 100 − 120 GPa, whereas Young's modulus of bone varies in a range of 4 − 30 GPa [1,2]. The difference between Young's moduli of the implant and bone lead to bone resorption and eventually implant loosening, so-called stress shielding [3]. The most commonly used material in bone replacement and repair is Ti-6Al-4V alloy, however, the alloying elements present in this alloy raises some clinical concerns such as neurological diseases and cytotoxic effects [4–6]. Therefore, novel Ti based alloys having low Young's modulus and having non-toxic and allergic-free elements are needed for bone and tissue applications [7].

The low Young's modulus Ti alloys have been developed with toxic-free elements, better mechanical properties, good corrosion resistance and excellent biocompatibility, by using β-stabilizing and biocompatible elements such as Nb, Mo, Ta, Zr, especially for orthopedic implant applications. Among these alloys, Ti-Nb based alloys draw a considerable attention for biomedical applications not only due to their non-toxicity, good corrosion behavior and biocompatibility, but also due to the presence of Nb that is reported as favorable for osteogenesis [8], cell adhesion, proliferation, and differentiation *in vitro* [9,10].

The spontaneously formed native passive oxide film on Ti and its alloys not only determines the corrosion resistance and release of metallic ions but also influences the biocompatibility of implants [11]. Accordingly, the corrosion behavior and biocompatibility of β-type Ti-xNb alloys are influenced by Nb stabilizing element in the passive film consisted of a mixture of protective oxides (TiO_2 and Nb_2O_5) [12]. For instance, Han et al. [13] reported a higher corrosion resistance for Ti-xNb (x = 5, 10, 15, and 20 wt%) alloys as compared to cp-Ti in 9 g/L NaCl solution at body temperature, due to a more protective natural oxide layer. Apart from the structure of the passive film, the microstructure also has an effect on the corrosion behavior [14]. Cremasco et al. [15] investigated the effect of water quenching and furnace cooling on the corrosion behavior of Ti-35Nb alloy by electrochemical impedance spectroscopy and potentiodynamic polarization. It was found that water quenching decreased the corrosion performance of the alloy due to its microstructure consisting of acicular martensitic phase. Bai et al. [16] studied the corrosion behavior of Ti-xNb (x = 45 and 55 wt.%) alloy and commercial Ti-11Mo-6 Zr-4Sn alloy in artificial saliva, and with addition of lactic acid and sodium fluoride solution. It was reported that the better corrosion resistance of Ti-xNb alloy over Ti-Mo-

* Corresponding author.
E-mail address: id6757@alunos.uminho.pt (I. Çaha).

https://doi.org/10.1016/j.corsci.2020.108488
Received 13 November 2019; Accepted 20 January 2020
Available online 22 January 2020
0010-938X/

Zr-Sn alloy in fluoridated saliva and fluoridated acidified saliva was due to the precipitation of acicular martensitic α″ phase in β phase for Ti-Mo-Zr-Sn alloy. Bai et al. [17] investigated the biocompatibility and corrosion behavior of Ti-45Nb alloy and cp-Ti in different solutions (simulated body fluid, modified Fusayama-Meyer artificial saliva, and fluoridated acidified artificial saliva) and found that the Ti-45Nb alloy presented better cell attachment and superior corrosion resistance than Ti due to the nobler behavior of Nb.

Most of the implants are exposed to tribocorrosion that is the degradation of material surfaces due to the simultaneous corrosion and mechanical interactions in a tribological contact [18]. For instance, tribocorrosion observed in hip joints since relative moments occur between femoral head and acetabular cup, as well, between femoral stem and cortical bone in the presence of body fluids [19]. More et al. [20] studied the tribocorrosion behavior of Ti-12.5Mo, Ti-13Nb-13Zr and Ti-29Nb-13Ta-4.6 Zr β-type titanium alloys and Ti-6Al-4Fe α + β-type Ti alloy under open circuit potential (OCP) and passive applied potential against ultra-high molecular weight polyethylene in Hank's balanced salt solution. The authors showed that the polyethylene presented low wear against β-type alloys and β-type alloys exhibited repassivation even during sliding, at passive potential and OCP.

Surface degradation of implants is one of the most important drawbacks for long-term implantation in the human body. In the last decade, many efforts have been spent for the development β-type Ti alloys, but the degradation behavior of these alloys are yet to be fully understood. Therefore, the present work aimed at studying the degradation behavior of Ti-15Nb and Ti-40Nb alloys in a simple physiological solution at body temperature, in comparison with Ti-6Al-4V as the most popular Ti alloy, by performing corrosion tests during prolonged times of immersion (up to 21 days), as well, by performing tribocorrosion tests against a hard and inert counter material.

2. Experimental procedure

2.1. Materials and processing

The raw materials used to produce alloys were cp-Ti (99.7 % purity, Sandinox Biometais, Brazil) and Nb (99.8 % purity, Brazilian Metallurgy and Mining Company). In order to remove superficial impurities, Ti and Nb raw materials were chemically cleaned in an HNO_3:HF (4:1) and HNO_3:HF:H_2O (2:2:1) solutions respectively. After chemical cleaning, the materials were immersed in acetone and cleaned in an ultrasonic bath for 20 min. These metals were melted by using an arc-melting furnace with water cooled copper crucible, non-consumable tungsten electrode under controlled atmosphere of argon. After that, the samples were subjected to heat treatment (1000 °C/24 h) in an ultra-vacuum furnace for homogenization. Then, the ingots with 15 wt. % and 40 wt.% of Nb were obtained by a hot-rolling process at 900 °C. After the hot-rolling, the samples were submitted to a new heat treatment of 8 h in vacuum to relieve the residual stress resulted from the machining procedure. In order to compare the results, commercial Ti-6Al-4V (VSMPO Tirus, US, ASTM B348, Grade 5) alloy was used in all tests.

Before microstructural characterization and microhardness measurements, samples were grinded down to 2400 mesh SiC paper, polished with colloidal silica suspension (Buehler, 0.02 μm) for 5 min in polishing machine (Aropol-2v, Arotec), and afterwards, etched with Kroll's reagent (%3 H F + %6 HNO_3 + %91 H_2O). For corrosion and tribocorrosion tests, samples were grinded with SiC papers down to 1200 mesh then cleaned in propanol and in distilled water for 10 min and 5 min respectively in ultrasonic bath. Before starting each test, samples were stored in a desiccator for 1 day.

2.2. Corrosion and tribocorrosion tests

Corrosion tests included of OCP measurements, potentiodynamic polarization and electrochemical impedance spectroscopy (EIS) were employed on 1.0 cm^2 of exposed area in 200 mL of saline solution (9 g/L NaCl) using Gamry Potentiostat/Galvanostat (model Reference-600+). A saturated calomel electrode (SCE) was used as reference electrode (RE), a Pt electrode was used as the counter electrode (CE) and the samples were used as working electrode (WE). Prior to potentiodynamic polarization, OCP employed till stabilization of native oxide film ($\Delta E < 60$ mV vs. SCE) and afterwards, the polarization scan was performed with 0.5 mV/s scan rate, starting at —0.25 V_{OCP} up to 1.5 V_{SCE}. EIS measurements were performed after 4 h, 1 day, 2 days, 4 days, 8 days, 16 days, and 21 days of immersion. Gamry Echem Analyst software was used for fitting the raw data and the quality of the proposed the electrical equivalent circuit (EEC) was evaluated by the goodness of fitting (χ^2). The potential of each sample was monitored during 30 min in test solution before each EIS measurement. The EIS measurements at OCP was carried out with a 10 mV of sinusoidal amplitude by scanning a range of frequencies from 10^5 Hz to 10^{-2} Hz with counting 7 points per frequency decade.

Tribocorrosion tests were performed at body temperature in saline (9 g/L NaCl) electrolyte using a tribometer (CETR-UMT-2) with pin-on-plate reciprocating sliding configuration. A two-electrode set-up was used where the samples were placed as WE against an alumina ball (10 mm in diameter, Ceratec) using a Gamry Potentiostat/Galvanostat/ZRA (model Reference-600). The tests were carried out under a reciprocating sliding frequency of 1 Hz, normal load of 1 N corresponding to maximum Hertzian contact pressures of 0.37 GPa, 0.27, and 0.42 GPa for Ti-15Nb, Ti-40Nb, and Ti-6Al-4V alloys respectively, and amplitude of 3 mm. Sliding started after stabilization of OCP ($\Delta E < 60$ mV vs. SCE) and continued during 30 min. Afterwards, the counter material was removed and OCP recorded for further 20 min in order to observe the repassivation.

All corrosion and tribocorrosion tests were triplicated on three different samples and all results were presented as the arithmetic mean ± standard deviation.

2.3. Characterization

Microstructures and chemical compositions were analyzed by optical microscope (Leica, DM2500), scanning electron microscope (SEM, EVO LS15 Carl Zeiss, with software SmartSEM), equipped with X-ray energy dispersive spectroscopy (EDS). Structural characterization of Ti-Nb alloys was performed by X-ray diffraction (XRD, DMAX-2100, Rigaku) and the quantification of phases estimated through the Rietveld's method by using the General Analyzer System Structure (GSAS) [22]. Vickers microhardness were determined by 5 identations performed randomly per sample using an Emcotest Durascan tester at a load of 9.8 N (1 kgf) during 15 s. The measurements of the elastic modulus were carried out in a dynamic manner using the Sonelastic® equipment (ATCP) based on ASTM-E1876 standard from 10 measurements, using the technique of excitation by impulse, with the samples placed in flexural vibration.

After each tribocorrosion test, the samples were cleaned by an ultrasonic bath in propanol and in distilled water for 10 min and 5 min respectively. The worn surfaces and collected wear debris were investigated by using FEG-SEM (FEI Nova 200) with backscattered (BSE) and secondary electron (SE) configuration, and analyzed with EDS. The total wear volume loss was determined by following the calculation procedure given elsewhere [21] through wear track profiles obtained by a surface profiler (Veeco, Dektak 150).

3. Results and discussion

3.1. Microstructural and mechanical characterization

Microstructural analysis revealed a homogenous distribution of Nb in both alloys, without any segregations (Fig. 1a and b). Nevertheless,

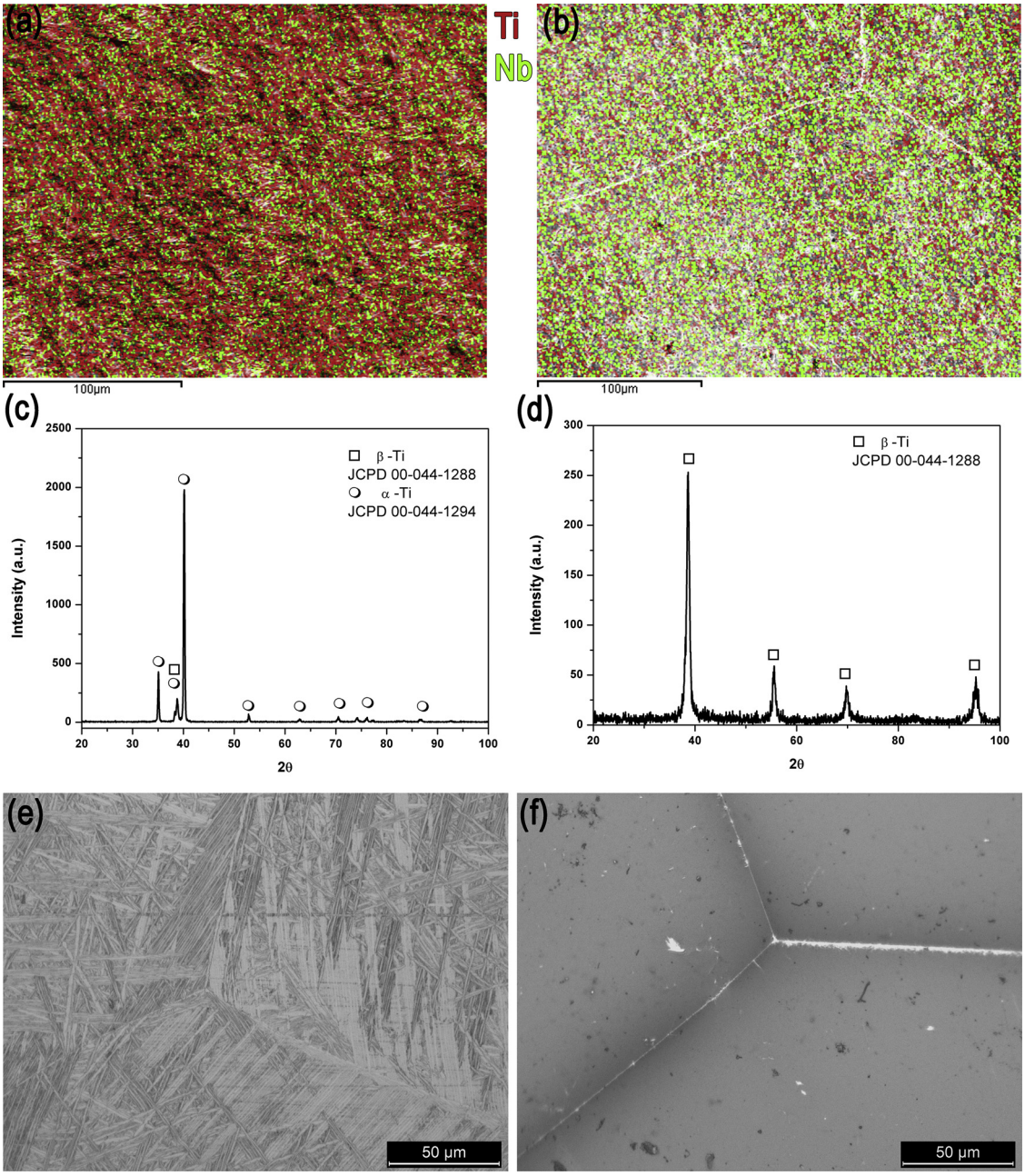

Fig. 1. EDS mapping (a, b), XRD spectra (c,d), and OM images (e, f) of Ti-15Nb and Ti-40Nb alloys respectively.

the amount of Nb in Ti matrix significantly affected the microstructure. XRD spectra (Fig. 1c and d) revealed that while Ti-15Nb alloy is composed of hexagonal-Ti (α-Ti) and body centered cubic-Ti (β-Ti) phases, which is composed by 56 % α-Ti - 44 % β-Ti, while 100 % β-Ti was calculated for the Ti-40Nb alloy. Microstructural analysis revealed typical Widmanstätten α + β structure for the Ti-15Nb alloy (Fig. 1e), whereas the Ti-40Nb alloy exhibited single-phase β microstructure (Fig. 1f). These microstructural differences also affected the mechanical properties, resulting with in a slight increase on hardness from the Ti-15Nb to the Ti-40Nb (249 ± 3 and 262 ± 5 $HV_{0.3}$, respectively) together with a significant decrease on the Young's modulus (88 ± 1 for the Ti15Nb and 51 ± 1 GPa for the Ti-40Nb). For comparison, it is worth to note that the hardness of the commercial Ti-6Al-4V alloy is 350 ± 5 $HV_{0.3}$, and its Young's modulus is known from the literature to be 112 GPa [1].

3.2. Corrosion behavior

Representative results of the potentiodynamic polarization tests are plotted in Fig. 2, together with a table depicting the corrosion potential ($E_{(i=0)}$) and the passivation current density (i_{pass}) at 0.5 V_{SCE}. A well-defined passivation plateau was observed for all alloys. The i_{pass} for the Ti-6Al-4V and Ti-15Nb were very similar and lower than the ones observed for the Ti-40Nb.

The corrosion behavior of passive materials is determined by the nature of the passive film spontaneously created on their surfaces. For Ti-Nb alloys it is reported that the passive film can be composed of TiO_2 and Nb_2O_5, while TiO_2, Al_2O_3, and V_2O_5 were found in the passive film of the Ti-6Al-4V alloy [23,24]. Nevertheless, the relative ratio of oxides is strongly dependent of the formation conditions and environmental history [24]. The Ti-15Nb and Ti-6Al-4V alloys presented very similar potentiodynamic polarization curves, whereas the curve of Ti-40Nb shifted slightly to the right indicating relatively accelerated kinetics.

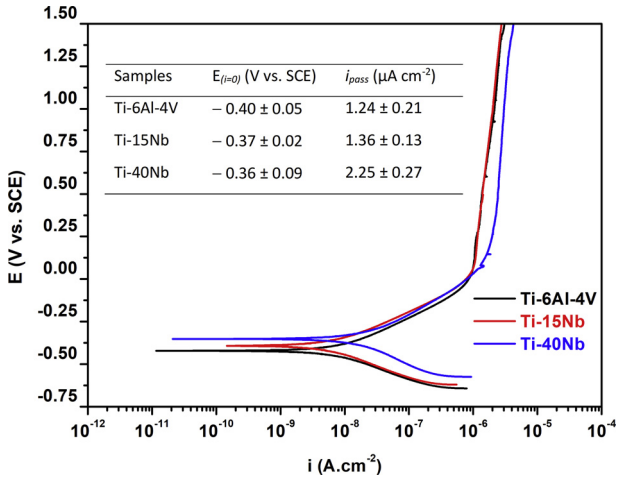

Fig. 2. Representative potentiodynamic polarization curves.

The i_{pass} values observed in this work are in accordance with those found by Gostin et al. [25] and Pilz et al. [12], who studied the potentiodynamic polarization of alloys in Ringer's solution and Tris-buffered saline (pH 7.6), respectively, where lower i_{pass} values were reported for the Ti-6Al-4V alloy than the Ti-40Nb alloy. However, an opposite trend was reported by Yilmaz et al. [26] after evaluating the corrosion behavior of powder injection molded α + β-type Ti-16Nb and Ti-40Nb alloys (mostly β phase but it was included a small amount of α phase) in simulated body fluid by using potentiodynamic polarization curves. The authors reported that the increased amount of Nb resulted with lower anodic current density values that was linked to the presence of Nb_2O_5 on the passive film that was indicated as more stable as compared to Al_2O_3 and V_2O_5 oxide compounds. These controversial results reported in the literature points that the effect of the nature of the passive film and the microstructure on the corrosion behavior of Ti-Nb alloys requires further electrochemical analysis.

The evolution of OCP through immersion time for the Ti-6Al-4V, Ti-15Nb, and Ti-40Nb alloys is presented in Fig. 3. The OCP values increased during the first 192 h (8 days) for all alloys, reaching similar electrochemical potentials (close to 0 V vs. SCE). Afterwards the values of Ti-15Nb and Ti-40Nb were remained relatively stable while the electrochemical potential of the Ti-6Al-4V alloy slightly increased reaching approximately 0.1 V_{SCE} at the end of the immersion period. The increase of OCP indicates a decrease in reactivity of the alloys and is usually associated with the thickening of the passive film in contact with the electrolyte, and/or to changes in the composition and structure of the passive film [23,27].

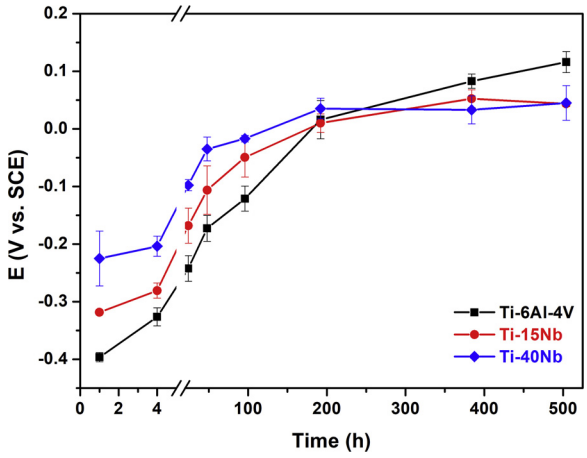

Fig. 3. Evolution of OCP during 21 days in 9 g/L NaCl.

The Bode diagrams of EIS spectra for 4 h, 2 days, 8 days, and 21 days of immersion are given in Fig. 4, together with the EEC used for simulation of the experimental data, representing a naturally formed oxide layer on the surface. All alloys presented the goodness of fitting below the 10^{-4} indicated a perfect agreement between the experimental data and the proposed EEC. At low and middle frequencies (10^{-2} — 10^{2} Hz), the phase angle values of all samples were close to —90° indicating a capacitive behavior of a compact layer whereas the constant |Z| values near 0° at high frequencies (10^{2} — 10^{5} Hz) presents the response of the electrolyte resistance.

Regarding the EEC, R_e is the electrolyte resistance, R_{ox} is the resistance of the native oxide film, and Q_{ox} is the constant phase element (CPE) indicating the deviation from an ideal capacitive behavior. The impedance of a CPE is given as $Z_{CPE} = [Y_0(jw)^n]^{-1}$, where Y_0 is CPE admittance in $\Omega^{-1}s^n$ cm^{-2} units, $j = \sqrt{-1}$ is the imaginary unit, $w = 2\pi f$ is the angular frequency in rad/s, and n is dimensionless number. The n values varies in $-1 \leq n \leq 1$ range and the CPE indicates an inductor, a resistor, and a capacitor behavior when $n = -1$, $n = 0$, and $n = 1$, respectively. The n value about 1 presents a non-deal capacitor behavior by CPE where it is related to a non-uniform current distribution due to the surface roughness and inhomogeneity.

Fig. 5 presents the R_{ox} and Q_{ox} evolution as function of immersion time. After 4 h of immersion, the average R_{ox} values were similar for all alloys. However, R_{ox} increased after 4 h, where the increase was more noticeable on Ti-6Al-4V alloy. On the other hand, Q_{ox} values decreased during the immersion time where Ti-15Nb alloy presented lower values as compared to the other alloys. As it is known, Q_{ox} is directly proportional to C_{ox} (capacitance of the natural oxide film), which is defined by $C = \frac{\varepsilon_0 \varepsilon_r A}{d}$, where ε_o is the vacuum primitivity ($\varepsilon_0 \approx 8.9\text{x}10^{-14} Fcm^{-1}$), ε_r is dielectric constant number, A is the exposure area, and d is the thickness of the oxide layer [28]. Therefore, the decrease on Q_{ox} during the immersion period may be linked with the thickening of the passive film, indicating an improvement on its quality [29].

The increase of R_{ox} for all alloys with the immersion period shows that the natural oxide film formed on the alloys became more resistive. The variations in the R_{ox} may be linked to the structural changes in the oxide layer and/or changes in the ionic or electrical conductivity of the oxide layer that may happen during the immersion period [30]. The average R_{ox} value of Ti-6Al-4V alloy was higher than that of the Ti-xNb alloys after 21 days of immersion, while the Q_{ox} values of the Ti-6Al-4V alloy evolved in between the values of Ti-15Nb and Ti-40Nb alloys. Normally, higher R_{ox} of Ti-6Al-4V is expected to give lower Q_{ox} value. This contradiction behavior of the Ti-6Al-4V alloy may be linked with the structure of the oxide film. It had been suggested in the literature that the oxide film naturally formed on the Ti-6Al-4V alloy surface is mainly composed by titanium oxides (mainly at the metal/oxide interface), however at the oxide/electrolyte interface this layer also contains aluminum oxides, along with vanadium oxides [31]. Metikoš-Huković et al. [32] stated that V is able to diffuse up to the Ti-6Al-4V alloy surface leading to the formation of V_2O_5 and other suboxides at the outermost surface. Moreover, vanadium oxide dissolution causes generation of vacancies in the oxide film [30,32]. However, these oxides are not as protective as TiO_2 films, thus the presence of these oxides leads to lower general quality of the passive film formed on Ti-6Al-4V alloy, particularly with the presence of chloride ions in the solution. This mechanism can also be understood by observing the variation of Q_{ox} values. While the all tested alloys showed similar trend with immersion time, the Ti-6Al-4V alloy presents higher values compared to Ti-15Nb that may be explained by the dissolution of vanadium and aluminum oxides. Cordeiro et al. [33] studied the corrosion behavior of Ti-Zr and Ti-Nb-Zr alloys in comparison with Ti and Ti-6Al-4V by using potentiodynamic polarization and EIS in SBF solution. The authors reported a higher corrosion resistance for α + β-type Ti-6Al-4V alloy than β-type Ti-35Nb-10Zr alloy and linked the difference with the less protective behavior of the passive film formed on β phase, as well as the higher hardness of Ti-6Al-4V alloy, that gave a better support to

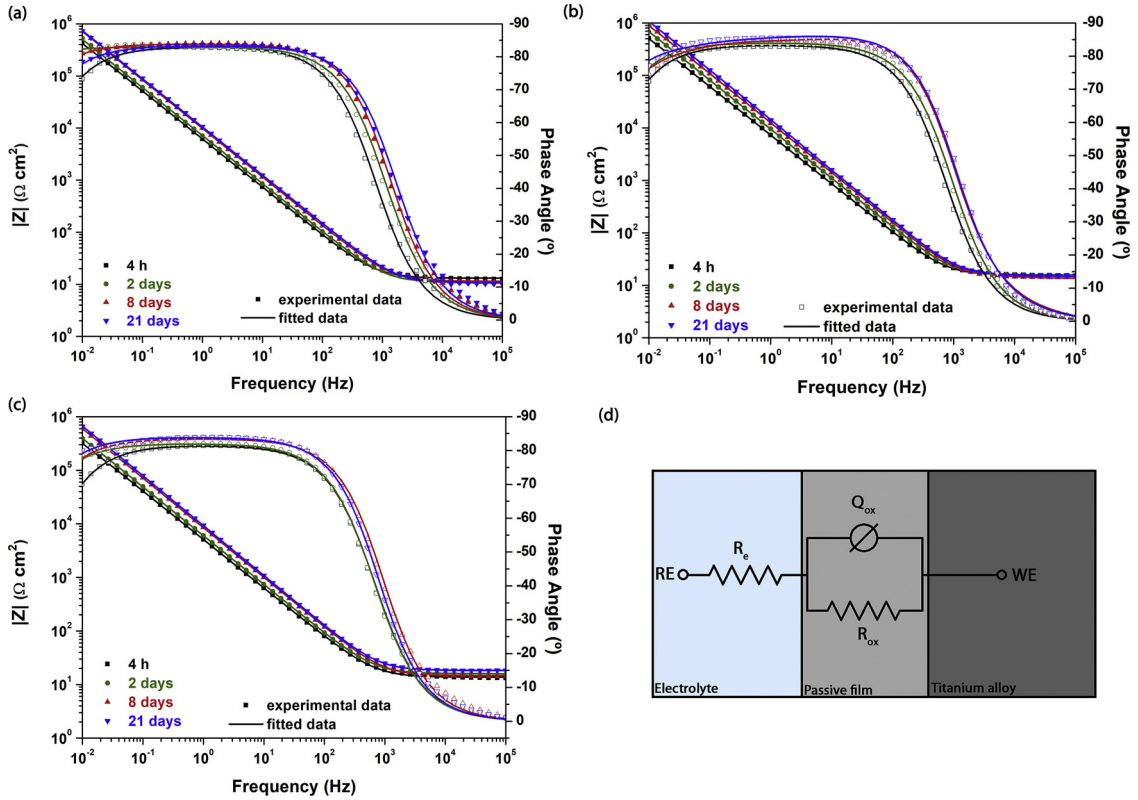

Fig. 4. Bode diagrams of a) Ti-6Al-4V, b) Ti-15Nb, and c) Ti-40Nb alloys in 9 g/L NaCl solution for different immersion times, together with d) the proposed EEC.

the oxide layer. This favorable effect of the hardness had also previously been reported by Cvijović-Alagić et al. [31] for Ti-6Al-4V and Ti-13Nb-13Zr alloys where higher hardness of the Ti–6Al–4 V alloy reported to support a thicker and more firmly adhered oxide layer as compared to a softer one. Regarding Ti-Nb alloys, lower Q_{ox} values of Ti-15Nb than Ti-40Nb alloy indicates the formation of a thicker and higher quality of oxide film, that requires further investigation particularly regarding its structure.

3.3. Tribocorrosion behavior

3.3.1. Worn surface analysis

In order to have an understanding on the tribocorrosion mechanism, worn surfaces and wear debris were characterized by SEM/EDS. Fig. 6 shows the wear track surfaces where parallel ploughing grooves and adhered/oxidized patches can be observed on all alloys. The fine aligned grooves indicated that abrasive wear occurred for all tested samples. Relatively denser oxidized patches were observed on Ti-6Al-4V surfaces as compared to both Ti-Nb alloys, as evidenced on the BSE images, that may be related with the higher hardness of the Ti-6Al-4V alloy that gave a better support to those patches, as previously explained by Lee et al. [34] on the wear behavior of β-type Ti-29Nb-13Ta-4.6 Zr and α + β-type Ti-6Al-4V alloys. On the other hand, Ti-6Al-4V produced finer and more regular blocky debris, whereas flake-like wear debris were observed on the Ti-Nb alloys. Moreover, the EDS spectra taken from the debris produced on Ti-6Al-4V exhibited higher oxygen peak compared to the ones obtained on Ti-Nb alloys. SEM images of the wear scars together with detached pieces from samples (insert images) on alumina ball and the EDS taken from the worn area are given in Fig. 6. EDS spectra suggested that material from the samples was transferred to the ball, clearly indicating the adhesive wear, that appeared to happen more on Ti-Nb alloys than Ti-6Al-4V alloy. The wear scar on the alumina ball slid against the Ti-40Nb alloy was relatively larger than the wear scar against the Ti-15Nb alloy, while the smallest

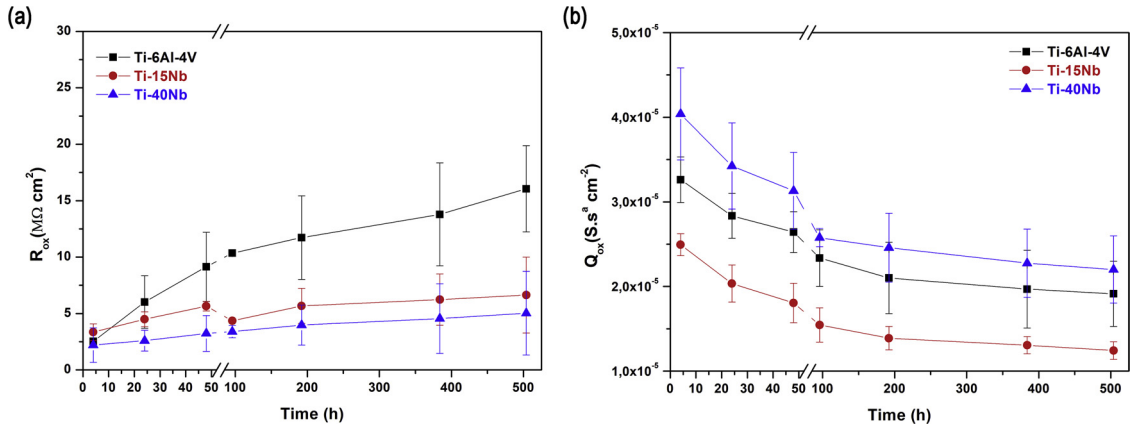

Fig. 5. Evolution of R_{ox} and Q_{ox} with immersion time.

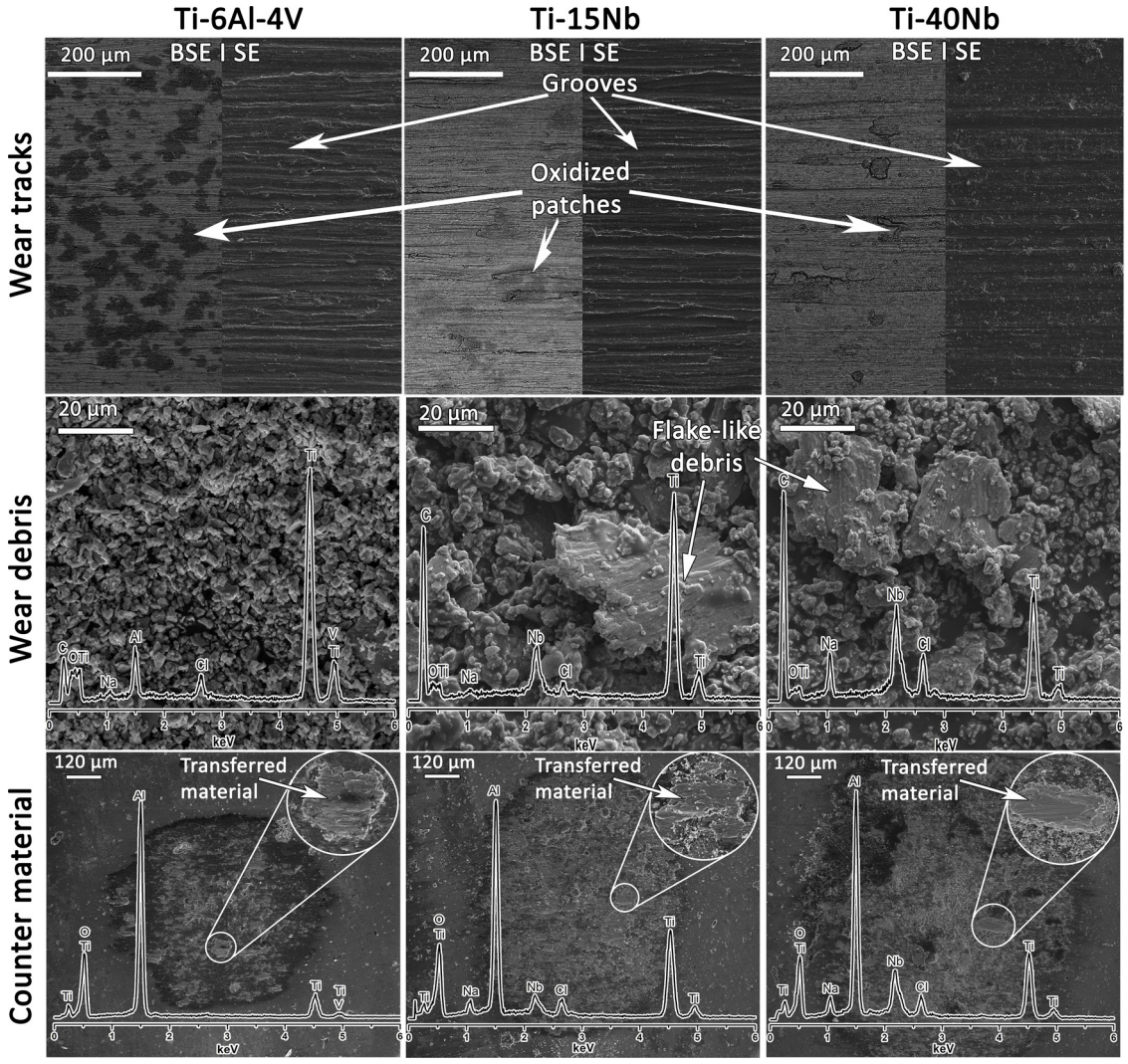

Fig. 6. SE and BSE-SEM wear track images, SE-SEM wear debris images together with corresponding EDS spectra, and wear scar images of counter material together with corresponding EDS spectra for Ti-6Al-4V, Ti-15Nb, and Ti-40Nb.

wear scar was obtained ball slid against the Ti-6Al-4V alloy.

Total wear volume loss and hardness of Ti-6Al-4V, Ti-15Nb, and Ti-40Nb alloy measured outside and inside the wear tracks are given in Table 1. The Ti-6Al-4V alloy presented significantly lower wear volume loss than both Ti-Nb alloys. Hardness of both Ti-Nb alloys did not vary significantly between the measurements taken on the worn and unworn surfaces whereas the hardness of Ti-6Al-4V alloy was significantly higher on the wear tracks. In addition to work hardening and the formation of the oxide patches, the plastic deformation at the subsurface of the wear track may led to lower wear volume loss for Ti-6Al-4V alloy. Fig. 7 shows BSE images of the subsurface of the wear track for all samples. A clear deformation zone was observed at the subsurface of Ti-6Al-4V alloy, while it was not observed evidences of deformation for both Ti-Nb alloys. It may be assumed that the higher stress level during sliding tended to produce a greater amount of dislocations in the subsurface zone and therefore led to a higher hardness. This subsurface deformation on Ti-6Al-4V wear track accompanied by strain hardening improved the resistance against wear. While Ti-6Al-4V and Ti-15Nb alloys were composed of α + β phase, the higher wear volume loss values of Ti-15Nb alloy can be explained by its lower hardness value and lack of strain hardening resulted from its microstructure. Significantly higher wear volume loss of Ti-40Nb alloy may be explained by the elevated contribution of delamination wear as evidenced by relatively rougher wear track surface and subsurface cracks (insert Fig. 7c). In delamination wear mechanism [35], it is assumed that the contact asperities have an increased plastic deformation during the relative movement, which accumulates during repetitive interactions. When the accumulated strain reaches a critical level, the subsurface cracks are nucleated below the wear track. When the crack becomes large enough, it fractures to yield flake-like debris (delamination). The similar subsurface cracks and flake-like wear debris behavior were reported by Lee et al. [36] for β-type Ti-29Nb-13Ta-4.6 Zr alloy that tested in Ringer's solution and air explained by dominantly adhesive and delamination wear mechanisms.

According to Archard's law, the wear volume loss of Ti-6Al-4V and Ti-Nb alloys should be correlated with their hardness [37]. However, this assumption does not take into account the role of hardening and oxides formation during sliding [38]. For instance, Yang et al. [39]

Table 1
Wear volume loss and hardness of samples outside and inside wear tracks.

Samples	Wear volume loss (mm^3)	Hardness (HV_1)	
		Outside wear track	Inside wear track
Ti-6Al-4V	0.006 ± 0.001	350 ± 8	423 ± 26
Ti-15Nb	0.016 ± 0.003	251 ± 7	269 ± 10
Ti-40Nb	0.041 ± 0.004	258 ± 8	265 ± 16

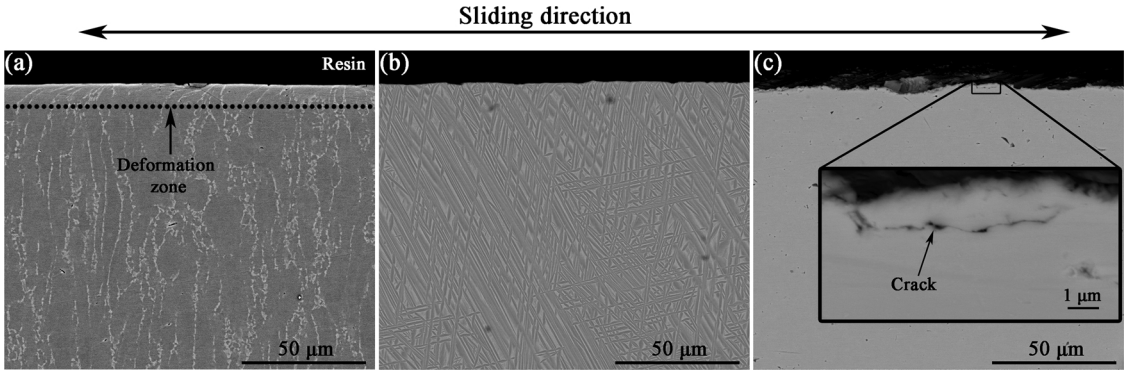

Fig. 7. Cross-sectional BSE SEM images of wear tracks parallel to the sliding direction for (a) Ti-6Al-4V, (b) Ti-15Nb, and (c) Ti-40Nb.

studied the tribocorrosion behavior β-type Ti-12Mo-6 Zr-2Fe alloy and α + β-type Ti-6Al-4V alloy in SBF and reported much higher wear volume loss values for Ti-12Mo-6 Zr-2Fe alloy as compared to Ti-6Al-4V alloy. The authors suggested that elevated wear volume loss was due to lack of strain hardening on β-type Ti alloys, that may also be the reason for more severe wear on fully β-type Ti-40Nb alloy observed in the present study.

3.3.2. Tribocorrosion analysis

The monitored OCP and coefficient of friction (COF) is given in Fig. 8. When sliding started, all alloys presented a sudden decrease on potentials (catholic shift) because of the mechanical damage given to the passive oxide film, showing an increase on the tendency to corrosion [20,40–42]. Afterwards, the potential values were slightly increased and then exhibited a steady state with oscillations resulting from repetitive repassivation-depassivation actions. When the sliding stopped, the OCP values were immediately increased close to the values observed before sliding due to the repassivation of the worn areas [20,40–42]. As can be seen on Fig. 8, no significant difference was obtained on the evolution of OCP between the testing alloys.

Regarding the evolution of COF, relatively stable values were observed during all sliding period, having average values of 0.38 ± 0.04, 0.45 ± 0.01, and 0.69 ± 0.02 for Ti-6Al-4V, Ti-15Nb, and Ti-40Nb alloys respectively. The higher COF of the Ti-40Nb alloy than those of the α + β-type Ti-15Nb and Ti-6Al-4V alloys may be linked with the elevated influence of the delamination wear and consequently, increased formation of flake-like wear debris. On the other hand, the formation of oxidized patches can significantly affect the COF values due to reduced contact between metal and counter material [43] that can explain the relatively lower COF values for the Ti-6Al-4V alloy (Fig. 6). Denser oxidized patches observed on the worn Ti-6Al-4V alloy surfaces may be explained by the higher hardness value of this alloy, since, as reported by Cvijović-Alagić et al. [31], the harder material is able to hold a thicker oxide layer more uniformly as compared to a softer material. Therefore, while the OCP evolution of both Ti-Nb alloy were similar, COF values were significantly affected by their microstructures.

3.3.3. Tribocorrosion mechanism

The wear process usually involves more than one simultaneous wear mechanism [44]. Fig. 9 schematically show the wear mechanism suggested for Ti-6Al-4V, Ti-15Nb and Ti-40Nb alloys. Abrasive and adhesive wear mechanisms were observed for all alloys although adhesive wear was more evident for Ti-Nb alloys. Also, the worn region of the Ti-6Al-4V alloy was characterized by a discontinuous tribolayer and subsurface plastic deformation. Finally, although both Ti-Nb alloys exhibited similar worn surface features, the Ti-40Nb alloy presented significantly higher wear loss and higher COF values, linked with formation of a more severe delamination wear, evidenced by elevated formation of subsurface cracks and flake-like wear debris.

4. Conclusion

Corrosion and tribocorrosion behavior of α + β-type Ti-15Nb and β-type Ti-40Nb alloys were investigated in compared with the

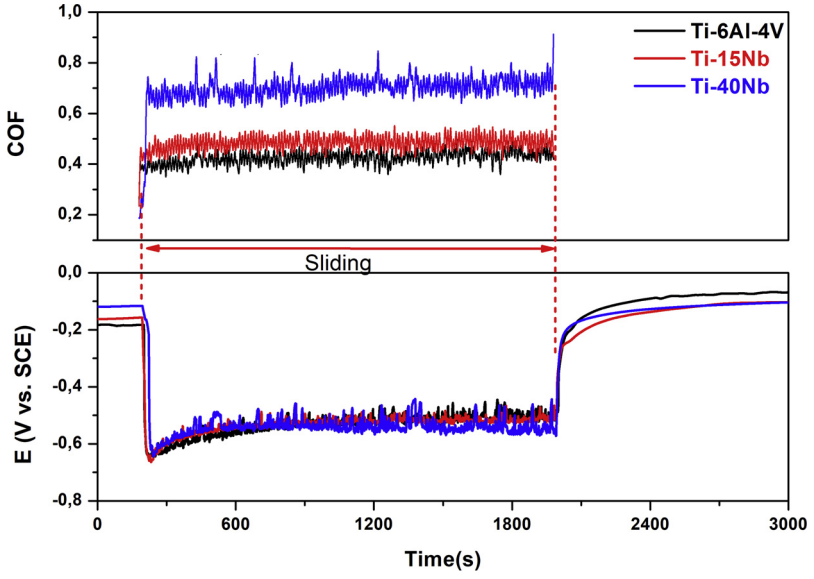

Fig. 8. OCP and COF evaluation of alloys in saline solution.

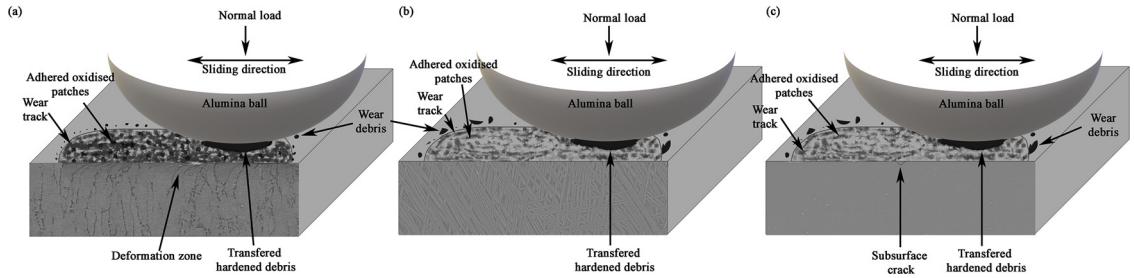

Fig. 9. Schematic illustration of wear mechanism of (a) Ti-6Al-4V (b) Ti-15Nb, and (c) Ti-Nb alloys.

commercial Ti-6Al-4V alloy. Although β-type Ti-40Nb alloy appears to be promising for osseointegrated implants, due to its lower Young's modulus (51 GPa), it exhibited lower corrosion resistance evidenced by lower resistance of the native oxide film and higher values of constant phase element through all immersion period suggestion a difference on the thickness and quality of the film. Ti-40Nb alloy also exhibited lower resistance to tribocorrosion particularly due to elevated influence of delamination wear. Therefore, these results showed that corrosion and tribocorrosion behavior of β-type Ti alloys should carefully be investigated and when necessary, suitable surface modification techniques should be considered before using them in load-bearing implant applications.

Declaration of Competing Interest

The authors declare that they have no known competing financial interests or personal relationships that could have appeared to influence the work reported in this paper.

Acknowledgements

This work is supported by FCTwith the reference project UID/EEA/04436/2019 and M-ERA-NET/0001/2015 (FAPESP proc. #2015/50.280-5), CNPq (307.279/2013-8) and FAPESP (2015/09.480-0). The authors would also like to acknowledge Prof. Graça Minas for the provision of the profilometry. I. Çaha is grateful for financial support through PhD grant under NORTE-08-5369-FSE-000012 project.

References

[1] M. Geetha, A.K. Singh, R. Asokamani, A.K. Gogia, Ti based biomaterials, the ultimate choice for orthopaedic implants – a review, Prog. Mater. Sci. 54 (2009) 397–425, https://doi.org/10.1016/j.pmatsci.2008.06.004.

[2] K. Miura, N. Yamada, S. Hanada, T.K. Jung, E. Itoi, The bone tissue compatibility of a new Ti-Nb-Sn alloy with a low Young's modulus, Acta Biomater. 7 (2011) 2320–2326, https://doi.org/10.1016/j.actbio.2011.02.008.

[3] A. Panigrahi, B. Sulkowski, T. Waitz, K. Ozaltin, W. Chrominski, A. Pukenas, J. Horky, M. Lewandowska, W. Skrotzki, M. Zehetbauer, Mechanical properties, structural and texture evolution of biocompatible Ti–45Nb alloy processed by severe plastic deformation, J. Mech. Behav. Biomed. Mater. 62 (2016) 93–105, https://doi.org/10.1016/j.jmbbm.2016.04.042.

[4] J.A. Davidson, A.K. Mishra, P. Kovacs, R.A. Poggie, New surface-hardened, low-modulus, corrosion-resistant Ti-13Nb-13Zr alloy for total hip arthroplasty, Biomed. Mater. Eng. 4 (1994) 231–243, https://doi.org/10.3233/BME-1994-4310.

[5] Y. Okazaki, E. Gotoh, Comparison of metal release from various metallic biomaterials in vitro, Biomaterials. 26 (2005) 11–21, https://doi.org/10.1016/j.biomaterials.2004.02.005.

[6] Y. Okazaki, Cytocompatibility of various metals and development of new titanium alloy for medical implant, Mater. Sci. Eng. A. 243 (1988) 250–256, https://doi.org/10.2320/materia.37.838.

[7] M. Niinomi, M. Nakai, J. Hieda, Development of new metallic alloys for biomedical applications, Acta Biomater. 8 (2012) 3888–3903, https://doi.org/10.1016/j.actbio.2012.06.037.

[8] H. Matsuno, A. Yokoyama, F. Watari, M. Uo, T. Kawasaki, Biocompatibility and osteogenesis of refractory metal implants, titanium, hafnium, niobium, tantalum and rhenium, Biomaterials 22 (2001) 1253–1262, https://doi.org/10.1016/S0142-9612(00)00275-1.

[9] E. Eisenbarth, D. Velten, M. Müller, R. Thull, J. Breme, Nanostructured niobium oxide coatings influence osteoblast adhesion, J. Biomed. Mater. Res. - Part A 79 (2006) 166–175, https://doi.org/10.1002/jbm.a.30823.

[10] M. Kushwaha, X. Pan, J.A. Holloway, I.L. Denry, Differentiation of human mesenchymal stem cells on niobium-doped fluorapatite glass-ceramics, Dent. Mater. 28 (2012) 252–260, https://doi.org/10.1016/j.dental.2011.10.010.

[11] A. Revathi, A. Dalmau, A. Igual, C. Richard, G. Manivasagam, Degradation mechanisms and future challenges of titanium and its alloys for dental implant applications in oral environment, Mater. Sci. Eng. C 76 (2017) 1354–1368, https://doi.org/10.1016/j.msec.2017.02.159.

[12] S. Pilz, A. Gebert, A. Voss, S. Oswald, M. Göttlicher, U. Hempel, J. Eckert, M. Rohnke, J. Janek, M. Calin, Metal release and cell biological compatibility of beta-type Ti-40Nb containing indium, J. Biomed. Mater. Res. - Part B Appl. Biomater. (2017) 1686–1697, https://doi.org/10.1002/jbm.b.33976.

[13] M.K. Han, J.Y. Kim, M.J. Hwang, H.J. Song, Y.J. Park, Effect of Nb on the microstructure, mechanical properties, corrosion behavior, and cytotoxicity of Ti-Nb alloys, Materials (Basel) 8 (2015) 5986–6003, https://doi.org/10.3390/ma8095287.

[14] F. Toptan, A.C. Alves, Ó. Carvalho, F. Bartolomeu, A.M.P. Pinto, F. Silva, G. Miranda, Corrosion and tribocorrosion behaviour of Ti6Al4V produced by selective laser melting and hot pressing in comparison with the commercial alloy, J. Mater. Process. Technol. 266 (2019) 239–245, https://doi.org/10.1016/j.jmatprotec.2018.11.008.

[15] A. Cremasco, W.R. Osório, C.M.A. Freire, A. Garcia, R. Caram, Electrochemical corrosion behavior of a Ti-35Nb alloy for medical prostheses, Electrochim. Acta 53 (2008) 4867–4874, https://doi.org/10.1016/j.electacta.2008.02.011.

[16] Y.J. Bai, Y.B. Wang, Y. Cheng, F. Deng, Y.F. Zheng, S.C. Wei, Comparative study on the corrosion behavior of Ti-Nb and TMA alloys for dental application in various artificial solutions, Mater. Sci. Eng. C 31 (2011) 702–711, https://doi.org/10.1016/j.msec.2010.12.010.

[17] Y. Bai, Y. Deng, Y. Zheng, Y. Li, R. Zhang, Y. Lv, Q. Zhao, S. Wei, Characterization, corrosion behavior, cellular response and in vivo bone tissue compatibility of titanium-niobium alloy with low Young's modulus, Mater. Sci. Eng. C 59 (2016) 565–576, https://doi.org/10.1016/j.msec.2015.10.062.

[18] F. Galliano, E. Galvanetto, S. Mischler, D. Landolt, Tribocorrosion behavior of plasma nitrided Ti-6Al-4V alloy in neutral NaCl solution, Surf. Coat. Technol. 145 (2001) 121–131, https://doi.org/10.1016/S0257-8972(01)01309-3.

[19] N. Diomidis, S. Mischler, N.S. More, M. Roy, Tribo-electrochemical characterization of metallic biomaterials for total joint replacement, Acta Biomater. 8 (2012) 852–859, https://doi.org/10.1016/j.actbio.2011.09.034.

[20] N.S. More, N. Diomidis, S.N. Paul, M. Roy, S. Mischler, Tribocorrosion behavior of β titanium alloys in physiological solutions containing synovial components, Mater. Sci. Eng. C 31 (2011) 400–408, https://doi.org/10.1016/j.msec.2010.10.021.

[21] Z. Doni, A.C. Alves, F. Toptan, J.R. Gomes, A. Ramalho, M. Buciumeanu, L. Palaghian, F.S. Silva, Dry sliding and tribocorrosion behaviour of hot pressed CoCrMo biomedical alloy as compared with the cast CoCrMo and Ti6Al4V alloys, Mater. Des. 52 (2013) 47–57, https://doi.org/10.1016/j.matdes.2013.05.032.

[22] R. Von Dreele, A. Larson, General Structure Analysis System (GSAS), Los Alamos Natl. Lab. Rep. LAUR, 2000, https://doi.org/10.1103/PhysRevLett.101.107006.

[23] A. Gebert, S. Oswald, A. Helth, A. Voss, P.F. Gostin, M. Rohnke, J. Janek, M. Calin, J. Eckert, Effect of indium (In) on corrosion and passivity of a beta-type Ti-Nb alloy in Ringer's solution, Appl. Surf. Sci. 335 (2015) 213–222, https://doi.org/10.1016/j.apsusc.2015.02.058.

[24] A.L.R. Ribeiro, P. Hammer, L.G. Vaz, L.A. Rocha, Are new TiNbZr alloys potential substitutes of the Ti6Al4V alloy for dental applications? An electrochemical corrosion study, Biomed. Mater. 8 (2013), https://doi.org/10.1088/1748-6041/8/6/065005.

[25] P.F. Gostin, A. Helth, A. Voss, R. Sueptitz, M. Calin, J. Eckert, A. Gebert, Surface treatment, corrosion behavior, and apatite-forming ability of ti-45Nb implant alloy, J. Biomed. Mater. Res. - Part B Appl. Biomater 101 B (2013) 269–278, https://doi.org/10.1002/jbm.b.32836.

[26] E. Yılmaz, A. Gökçe, F. Findik, Ho.O. Gulsoy, Metallurgical properties and biomimetic HA deposition performance of Ti-Nb PIM alloys, J. Alloys Compd. 746 (2018) 301–313, https://doi.org/10.1016/j.jallcom.2018.02.274.

[27] S.L. Assis, I. Costa, Electrochemical evaluation of Ti-13Nb-13Zr, Ti-6Al-4V and Ti-6Al-7Nb alloys for biomedical application by long-term immersion tests, Mater. Corros. 58 (2007) 329–333, https://doi.org/10.1002/maco.200604027.

[28] M.E. Orazem, B. Tribollet, Electrochemical Impedance Spectroscopy, (2008), https://doi.org/10.1002/9780470381588.

[29] M. Aziz-Kerrzo, K.G. Conroy, A.M. Fenelon, S.T. Farrell, C.B. Breslin, Electrochemical studies on the stability and corrosion resistance of titanium-based implant materials, Biomaterials 22 (2001) 1531–1539, https://doi.org/10.1016/S0142-9612(00)00309-4.

[30] A.K. Shukla, R. Balasubramaniam, S. Bhargava, Properties of passive film formed on

CP titanium, Ti – 6Al – 4V and Ti – 13. 4Al – 29Nb alloys in simulated human body conditions, Intermetallics 13 (2005) 631–637, https://doi.org/10.1016/j.intermet.2004.10.001.
[31] I. Cvijović-Alagić, Z. Cvijović, S. Mitrović, V. Panić, M. Rakin, Wear and corrosion behaviour of Ti-13Nb-13Zr and Ti-6Al-4V alloys in simulated physiological solution, Corros. Sci. 53 (2011) 796–808, https://doi.org/10.1016/j.corsci.2010.11.014.
[32] M. Metikoš-Huković, A. Kwokal, J. Piljac, The influence of niobium and vanadium on passivity of titanium-based implants in physiological solution, Biomaterials 24 (2003) 3765–3775, https://doi.org/10.1016/S0142-9612(03)00252-7.
[33] J.M. Cordeiro, T. Beline, A.L.R. Ribeiro, E.C. Rangel, N.C. da Cruz, R. Landers, L.P. Faverani, L.G. Vaz, L.M.G. Fais, F.B. Vicente, C.R. Grandini, M.T. Mathew, C. Sukotjo, V.A.R. Barão, Development of binary and ternary titanium alloys for dental implants, Dent. Mater. 33 (2017) 1244–1257, https://doi.org/10.1016/j.dental.2017.07.013.
[34] Y.S. Lee, M. Niinomi, M. Nakai, K. Narita, K. Cho, Predominant factor determining wear properties of β-type and (α + β)-type titanium alloys in metal-to-metal contact for biomedical applications, J. Mech. Behav. Biomed. Mater. 41 (2015) 208–220, https://doi.org/10.1016/j.jmbbm.2014.10.005.
[35] N.P. Suh, An overview of the delamination theory of wear, Wear 44 (1977) 1–16, https://doi.org/10.1016/0043-1648(77)90081-3.
[36] Y. Lee, M. Niinomi, M. Nakai, K. Narita, K. Cho, Differences in wear behaviors at sliding contacts for β-type and (α + β)-Type titanium alloys in ringer' s solution and air, Mater. Trans. 56 (2015) 317–326.
[37] J.F. Archard, Contact and rubbing of flat surfaces, J. Appl. Phys. 24 (1953) 981–988, https://doi.org/10.1063/1.1721448.
[38] A. Ball, On the importance of work hardening in the design of wear-resistant materials, Wear 91 (2) (1983) 201–207, https://doi.org/10.1016/0043-1648(83)90254-5.
[39] X. Yang, C.R. Hutchinson, Corrosion-wear of β-Ti alloy alloy TMZF (Ti-12Mo-6Zr-2Fe) in simulated body fluid, Acta Biomater. 42 (2016) 429–439, https://doi.org/10.1016/j.actbio.2016.07.008.
[40] V.G. Pina, A. Dalmau, F. Devesa, V. Amigó, A.I. Muñoz, Tribocorrosion behavior of beta titanium biomedical alloys in phosphate buffer saline solution, J. Mech. Behav. Biomed. Mater. 46 (2015) 59–68, https://doi.org/10.1016/j.jmbbm.2015.02.016.
[41] J. Ureña, S. Tsipas, A.M. Pinto, F. Toptan, E. Gordo, A. Jiménez-Morales, Corrosion and tribocorrosion behaviour of β-type Ti-Nb and Ti-Mo surfaces designed by diffusion treatments for biomedical applications, Corros. Sci. (2018) 0–1, https://doi.org/10.1016/j.corsci.2018.06.024.
[42] I. Golvano, I. Garcia, A. Conde, W. Tato, A. Aginagalde, Influence of fluoride content and pH on corrosion and tribocorrosion behaviour of Ti13Nb13Zr alloy in oral environment, J. Mech. Behav. Biomed. Mater. 49 (2015) 186–196, https://doi.org/10.1016/j.jmbbm.2015.05.008.
[43] Z. Doni, A.C. Alves, F. Toptan, A.M. Pinto, L.A. Rocha, M. Buciumeanu, L. Palaghian, F.S. Silva, Tribocorrosion behaviour of hot pressed CoCrMo–Al2O3 composites for biomedical applications, Tribol. - Mater. Surfaces Interfaces 8 (2014) 201–208, https://doi.org/10.1179/1751584X14Y.0000000078.
[44] G.W. Stachowiak, A.W. Batchelor, Engineering Tribology, fourth edition, (2013), https://doi.org/10.1016/C2011-0-07515-4.